A Passive Wireless Sensor Network for Temperature Mapping Inside a Shielded Coaxial Enclosure

S. Lopez-Soriano, I. P. Spassovsky , J. Parron, and G. Marrocco

***Abstract*— This contribution addresses the electromagnetic feasibility of the wireless temperature monitoring inside a coaxial cavity resembling a portion of a high-power high-frequency Cyclotron Auto-Resonance Maser (CARM) for plasma heating in the new generation of DEMO TOKAMAK machines. The scenario is investigated as a potential communication channel for a UHF RFID sensor network where cavity probes are used to both excite the coaxial cavity and to collect the temperature data scattered back by sensor antennas. By using a theoretical near-field analysis of a simplified model of the cavity and of the reader/sensor devices it is demonstrated that a two-probes architecture is suitable to interact with more than N=16 equally spaced RFID temperature sensors (having power sensitivity of -8.3dBmW) over the surface of a 0.5 m tube by using less than 20dBmW power emitted by the reader. The theoretical results are corroborated by experimental data with a mock-up of the cavity and realistic prototypes of miniaturized RFID radio-sensors and excitation probes.**

***Index Terms* — Wireless RFID sensor network, backscattering modulation, Electron vacuum tubes, temperature mapping.**

I. Introduction[1]

The Cyclotron Auto-resonance Maser (CARM) is an ongoing research project [1] aimed at the development of a Mega-Watt single beam 250 GHz oscillator in continuous wave (CW) operation for plasma heating and current drive in the future DEMO TOKAMAK machine [2]. The temperature variation of the cavity wall is crucial as the change of few degrees could dramatically affect its quality factor and would hence push the oscillator out of resonance conditions. At this purpose, the main cylindrical resonant cavity (Fig. 1) is held inside a second cooling cylinder where vacuum is enforced. The surface temperature must be precisely controlled at many points on the external surface of the CARM camera inside a coaxial-like environment.

Conventional measurement systems based on wired probes are expected to be problematic due to the small available space for cable allocation between the two conductors of the coaxial cavity. Thus, a less invasive and versatile architecture could comprise a wireless monitoring system involving cable-less sensors suitable to be interrogated by electromagnetic waves that are excited into the cavity by a probe. However, batteries are not recommended due to the small available space, to the need of reducing additional losses and to avoid risky manual maintenance. Instead, the interaction between sensors and the reading node should more conveniently exploit a backscattering modulation link where the sensors are pure passive devices that send back their information by modulating the interrogation field they reflect. One of the natural candidate technology is the Radiofrequency Identification (RFID) in the ultrahigh-frequency (UHF) band that is currently evolving from assessed logistics applications toward more advanced sensing and diagnostics in the Industrial Internet of Things [3]-[6]. Passive RFID sensing tags are compact and generally less expensive than more conventional local powered sensor nodes. One of the most critical features of battery-less RFID sensors is generally their modest read range (a couple of meters at most), that is affected by the propagation loss and degrades along with the reduction of the size of the radio sensor. The scenario under test has a rather limited extension and, above all, the electromagnetic interactions would take place inside an extremely low-loss cavity with a potential great benefit to the communication reliability [7]. Finally, the RFID protocol is capable to handle the concurrent interrogation of a multitude of tags so that a dense spatial temperature sampling of the interior should be possible. Therefore, a passive RFID sensor network looks a suitable approach to the problem even if some challenges still exist, such as the extreme antenna miniaturization and the cohabitation of a grid of closely spaced sensors with the cavity resonances.

The RF propagation through cylindrical heating, ventilation, and air conditioning (HVAC) ducts has been already studied in [8]. Later on, the characterization of the RF propagation in cylindrical metal pipes was formulated in [9] for passive RFID systems. The readability percentage of a commercial dipole-like tag inside a HVAC duct was then experimentally tested in [7]. A different application is proposed in [10] consisting in a VLF RFID system for monitoring the oil and gas quality.

Overall, the few available papers [7]-[12] refer to a scenario of merely two elements, namely, a transmitter/receiver and an identification tag. However, in a denser tag network, the fields inside the structure may not

[1] Paper submitted on January 2018. S. Lopez-Soriano and J. Parron are with Universitat Autònoma de Barcelona, Bellaterra, Spain; G. Marrocco is with the University of Roma Tor Vergata, Itlay; I. Spassowsky is with ENEA, Frascati (RM), Italy.

be expressed as the sum of a few propagating modes. In addition, at the purpose to provide accurate results, the scattered field produced by reflections on the network elements must be considered.

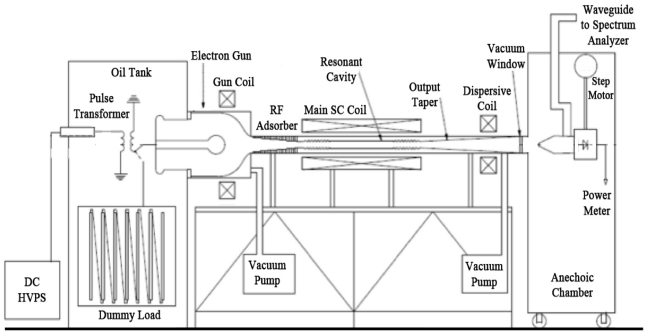

Fig. 1: Simplified sketch of the Cyclotron Auto-resonance Maser (CARM) [2] with indication of the resonant cavity to be thermally monitored.

This paper describes a feasibility study and a preliminary experimentation for the temperature mapping inside a coaxial cavity based on the backscattering modulation. The goal is to demonstrate the possibility to interrogate multiple RFID sensor tags inside the coaxial volume and to determine the lower bound of the reader's power that is required to establish a robust communication in case of different alignments and densities of tags. Following the description and the formalization of the near-field scenario, (Section II), excitation probes and miniaturized RFID temperature sensors are introduced (Section III), with specific applicability over metallic surfaces. After the fabrication of some prototypes, the overall sensor network is validated (Section IV) by means of a reference mockup of the CARM camera to corroborate the theoretical/numerical findings. Finally, two examples of temperature measurements are provided in section V.

II. The Sensor Network Components

As at time being, the CARM design is still in the preliminary stage and several geometrical parameters still need to be fixed, we considered a simplified model that is also suitable to be fabricated for a preliminary test of the proposed sensor network. The CARM mockup (Fig. 2) comprises two concentric metallic cylinders the main camera C_1, whose temperature on the external surface has to be monitored and the shielding and air-cooling camera C_2. Their front and back faces are closed by conducting plates thus forming a coaxial cavity. Moreover, the length of cavity (L = 484 mm) is roughly 3λ/2 at the UHF-RFID frequencies and hence the cavity will host a resonant mode. This specific boundary condition can be considered as a worst case as it will induce a standing wave of the internal field and hence there will be the challenge in the interrogation of those sensors placed close to the field nulls.

The proposed UHF RFID sensing network, to be deployed outside C_1, is conceived to operate in the UHF European band (865-868 MHz) and includes an RFID reader connected to a source probe antenna. The probe excites the interrogation field inside the coaxial cavity to activate the set of sensors on the surface of C_1. Given the size of the cavity, the maximum height of the sensing tags should be around 15 mm.

A. Reader's antenna for excitation of the coaxial cavity

Unlike cylindrical pipes considered in [7]-[10], coaxial structures allow to propagate a TEM mode that will be the only mode propagating up to 1.3 GHz (the cut off of TE_{11} mode) [14]. Accordingly, all the antennas (excitation probes and RFID sensors) must be oriented along the radial direction to enforce the best coupling with the TEM mode.

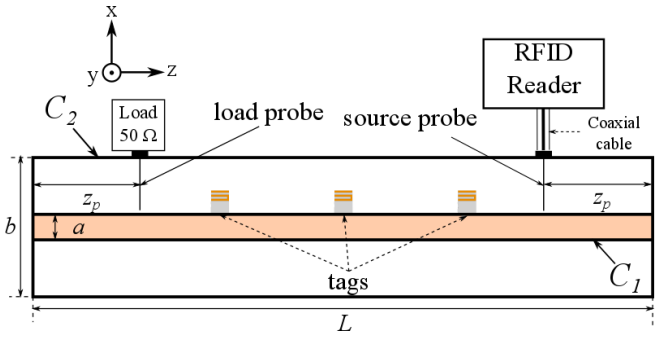

Fig. 2: Scheme of the reference coaxial cavity and the RFID sensor network. Sizes in [mm]: L = 484, a = 27, b = 108, probe-termination distance z_p = 70.

The considered excitation probes consist in shaped monopoles (Fig. 3) of λ/4 length at 867MHz. The monopole is folded twice to facilitate the placement inside the cavity. A foam holder (closed-cell PVC, ε_r = 1.55, σ = 6·10-4 S/m) is used to fix the probe to the cavity. In order to dump the cavity resonance, a second loading probe, connected to a 50 Ω load, is placed at the end of the cavity (Fig. 2). Numerical simulations with the Method of Moments [15] verified that (Fig. 4) this arrangement ensures the absence of sharp blind zones preventing the activation of RFID link. Sensing tags can be therefore placed freely all along the C_1 surface.

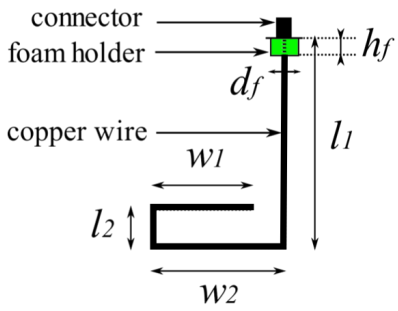

Fig. 3: a) Folded probe antenna for cavity excitation and tag interrogation. Size in [mm]: l_1 = 39, l_2 = 5, w_1 = 25, w_2 = 20, $l_{tot} = l_1 + l_2 + w_1 + w_2$=83,

wire radius = 0.5, d_f = 5 mm and h_f = 5 mm are respectively the diameter and height of the cylindrical foam holder.

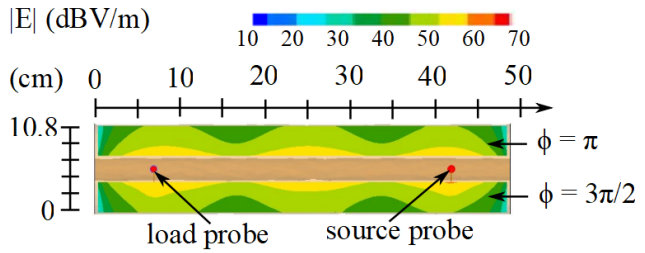

Fig. 4: Numerical simulation of the electric field magnitude (dBV/m) for φ = π and 3π/2 planes excited by a small probe with a second probe terminated onto a matched load

B. Radio Sensors

The RFID sensors include the EM4325-V11 microchip transponder [17] (power threshold P_S = -8.3 dBm) capable of combined identification and temperature sensing in the range -40°C < T < 65°C with resolution 0.25°C. Following the calibration in [18], the accuracy of this sensor is 0.18°C thus fully masked by its resolution. The chip impedance declared by the manufacturer is {23.3-j145, 17.6-j113, 14.5-j95} Ω at frequencies {866, 915, 953} MHz, respectively. These values were interpolated in the simulations for the intermediate frequencies.

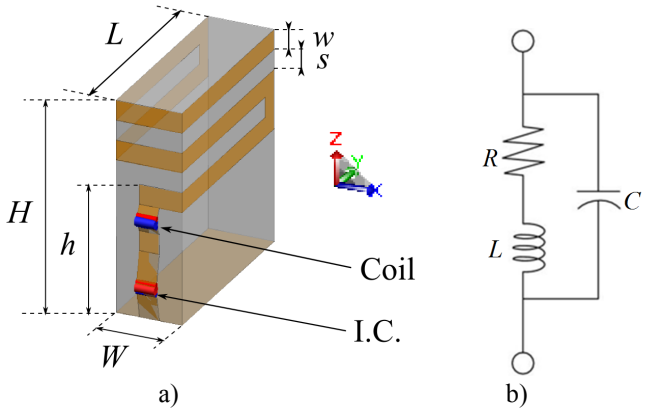

Fig. 5 a) Miniaturized sensor antenna layout, size in [mm]: W = 5, L = 15, H = 16, h = 10, w = 1.5, s = 1.5. b) Equivalent model of the lumped inductor: L=47 nH, C=64 fF and R=4.72 Ω.

The tag antenna (Fig. 5) consists of a 3D meandered monopole trace wrapped around the surface of a PVC (Polyvinyl Chloride, ε_r = 2.3, tanδ = $2 \cdot 10^{-4}$) foamboard parallelepiped. The antenna was conjugate matched to the chip at 867 MHz. The antenna reactance is then controlled by a lumped inductor (47 nH) connected in series with the chip. The numerical model of the inductor includes the parasitic effects and the self-resonance and losses of the coil through the RLC equivalent circuit in Fig. 5(b), whose parameters were derived from the datasheet [13] of the inductor. The resulting antenna has the maximum size of just one tenth of wavelength.

The power transfer coefficient τ of the tag is numerically evaluated at 47 positions (at 1cm step) over the external surface of cylinder C_1 (Fig. 6.(a)). The bandwidth corresponding to τ >-3dB is equal to 50 MHz for most of the considered positions (except for those at the borders, where the internal field reduces due to the presence of the short circuit terminations as in Fig. 4). The distribution of the power transmission coefficient along the cavity is almost uniform and hence it is rather insensitive to the inhomogeneity of the internal field.

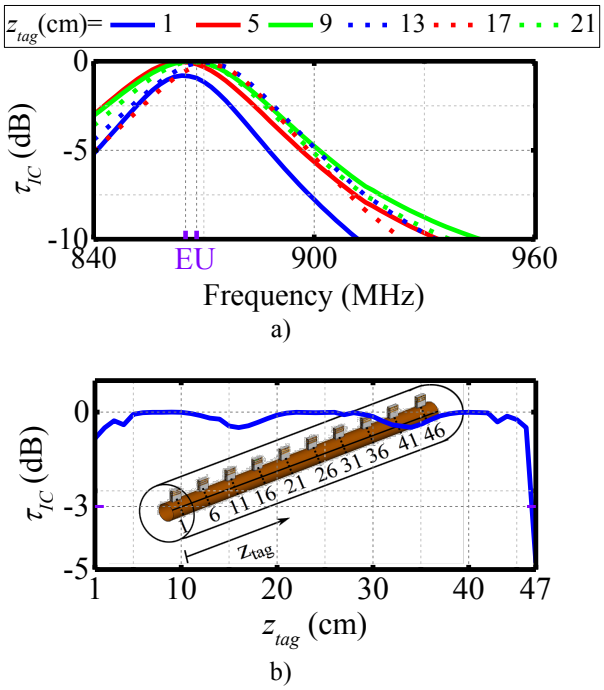

Fig. 6: a) Simulated power transfer coefficient of the tag a) vs. frequency and at some positions inside the cavity and b) vs. the position inside the cavity @867 MHz.

III. System Analysis

To quantify the performance and potential cut-off of the proposed wireless sensor network inside the cavity, several arrangements of RFID tags are here considered concerning their number N and their density.

As the reader-tag communication takes place in a shielded enclosure, the interactions among the components take place in the near field and accordingly the Friis equation [14] does not apply. A first-order model of the RFID link within the cavity assumed N two-port networks, each referred to a reader-tag link, while the other N-1 tags are anyway present in the simulation and connected to the microchip load. The reader-tag link inside the camera is then modelled by the *Transduction Power Gain* (G_T) [14], which is defined as the ratio between the power ($P_{R\to t}$) received by the chip and the output available power ($P_{av,R}$) from the reader. It can be calculated as:

$$G_T = \frac{P_{R\to t}}{P_{\text{av},R}} = \frac{\left(1-|\Gamma_G|^2\right)|S_{21}|^2\left(1-|\Gamma_L|^2\right)}{\left|\left(1-S_{11}\Gamma_G\right)\left(1-S_{22}\Gamma_L\right)-S_{12}S_{21}\Gamma_G\Gamma_L\right|^2} \quad (1)$$

where Γ_G is the reflection coefficient at the source, Γ_L is the reflection coefficient at the load and $[S_{ij}]$ are the entries of the *S*-parameters matrix of the two-port network describing the probe-tag interaction. The minimum reader's power P_{to} $=min(P_{av,R})$ required to activate the chip, say the "*turn-on power*", is hence evaluated by enforcing $P_{R\to t}=P_s$ (sensitivity of the chip) and accordingly

$$P_{to} = \frac{P_s}{G_T} \quad (2)$$

The turn-on power is an effective performance parameter useful to quantify the feasibility of the proposed architecture as its upper bound is typically limited to 30 dBmW in state of the art COTS[2] RFID readers.

Fig. 7 shows the distribution of the electric field inside the camera for *N*= {4, 8 and 16} sensors, each connected to the microchip impedance, and placed along a line at a same uniform distance or according to an interleaved configuration. Owing to the small available spaces in between the two tubes, the field distribution is strongly disturbed by the presence of multiple tags and the symmetry in the empty camera (Fig. 4) is broken. In all the configurations, the electric field close to the sensor reduces as moving far away from the exciter and accordingly the sensors will collect less and less power. Moreover, the field distribution becomes more concentrated around the sensors as their density increases. The corresponding turn-on powers versus the position of the tags (Fig. 8) exhibit a roughly linear behaviour (in dB) with the position of the tag (slope γ i.e. the power attenuation, is reported in Tab. 1). The minimum power that the reader should emit for the interrogation of all the tags increases along with the number of sensors. For a small number of tags (*N*<=8), the values of the turn-on power are rather similar for the linear and interleaved configurations (attenuation slopes close to γ=0.5 in both the cases). For a denser set of sensors (ex. *N*=16), instead, the linear displacement configuration looks more efficient since the required power to activate all the tags is slightly lower with respect to the interleaved displacement (attenuation slope 0.61 against 0.72) .

In case of many sensors (*N*=16), some of them placed at the farthest distance from the exciter, will require a reader's power approaching or even exceeding the capability of current readers (say for instance 30dBmW). A possible mitigation of this limit is discussed in the conclusions.

[2] Commercial Off The Shelf.

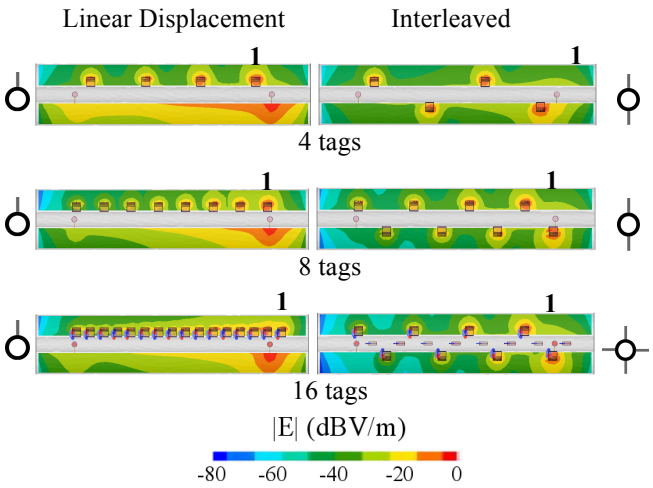

Fig. 7 : Simulations of the normalized electric field at 867 MHz inside the cavity for *N*= {4, 8, 16} RFID tags in different arrangements when the reader emits 30dBmW.

Tab. 1 Slope γ of the turn-on power distribution versus the position of the sensors and for various arrangements of them

N	Linear displacement [W/cm]	Interleaved [W/cm]
4	0.23	0.26
8	0.49	0.5
16	0.36	0.58

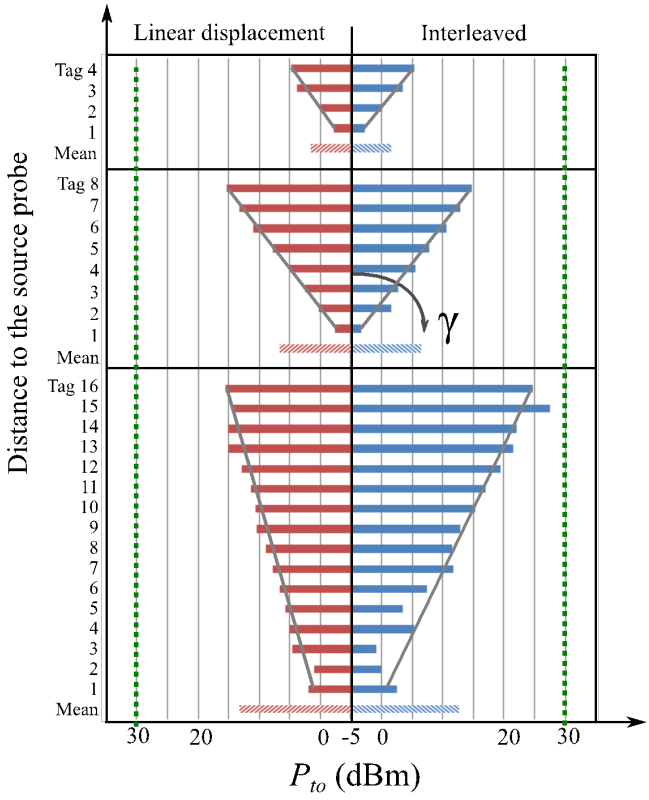

Fig. 8: Summary of the numerically estimated turn-on powers, at 867 MHz, of the RFID sensors for the arrangements in the Fig. 7. Dashed lines indicate the typical maximum output powers of state of the art readers.

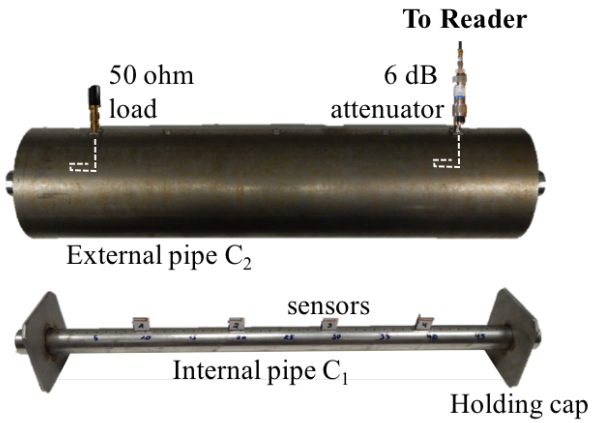

Fig. 9: External and internal view of the mockup of the coaxial cavity.

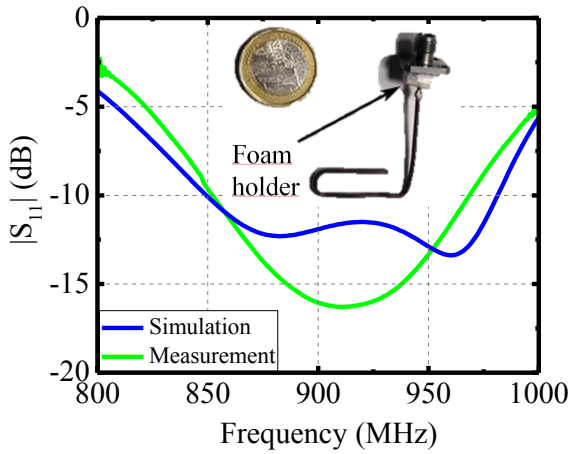

Fig. 10: Manufactured cavity probe and its power reflection coefficient inside an empty cavity when the second probe was terminated to 50 Ohm.

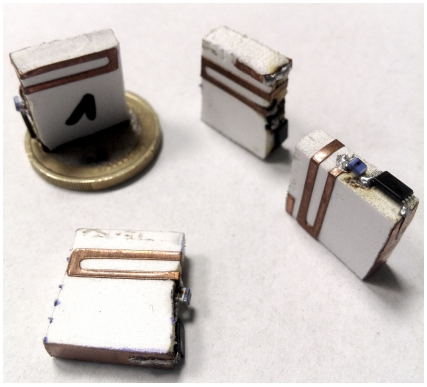

Fig. 11: Manufactured prototypes of the temperature sensor tags.

IV. EXPERIMENTAL VALIDATION

The proposed telemetry system is evaluated inside a cavity mock up (Fig.9) made by two still hollow cylinders having the same size of the simulated ones. Pipes are concentric arranged to form a coaxial cavity by means of two steel caps, each provided with a circular aperture in the middle to host the internal cylinder. Two small holes were then drilled on the curved surface of the smaller pipe for the mounting of the probes. Overall, the volume in the between the two cylinders forms the needed shielded coaxial enclosure which is fully decoupled from the internal volume of cylinder C_1. Thus, all the electromagnetic interactions will take place inside the coaxial enclosure and the interior of the smaller cylinder is communicating with the outside for the implementation of the heating experiments described later on. The meandered probe monopoles were fabricated by manually shaping a 1 mm copper wire (Fig. 10) then soldered to a SMA connector and supported by a foam disk around the connector pin to facilitate the mounting inside the coaxial cavity. The measured power reflection coefficient satisfactorily compares with the simulation (also including the foam spacer). The experimental -10dB bandwidth is 850-950 MHz thus covering the worldwide UHF RFID band.

The RFID sensors (Fig. 11) were manufactured with adhesive copper, by means of a digital controlled cutter, and then assembled over the PVC layer. The substrate was cut manually whereby the tags presented slightly different substrate dimensions and therefore they required individual fine tuning after fabrication by iteratively trimming the monopole tip that was hence originally fabricated longer than the corresponding numerical design.

For the characterization of the electromagnetic responses of the sensor inside the cavity, the excitation probe was connected to the ThingMagic M5e reader [19] driven by proprietary software. The turn-on power of each reader-tag link was hence evaluated by increasing the power emitted by the reader until the tag starts responding. The procedure is repeated for discrete frequencies within the worldwide UHF RFID band.

By means of a preliminary measurement with a single tag, it was proved that the turn-on power is lower than the minimum selectable output power from the reader, therefore, a 6 dB attenuator was placed between the probe and the reader (Fig. 9).

A. Single tag in variable positions

An example of measured turn-on power (P_{to}) of a tag inside the cavity, over C_1 cylinder, is visible in Fig. 12 and compared with simulations. The response of the tag exhibits a frequency shift of about 20MHz probably due to the imperfection of the manual manufacturing of the tag.

The RFID link was qualified by numerically and experimentally estimating the reflection coefficient (Fig.13(a)) of the probe and the turn-on power of the tag (Fig. 13(b)) when the it was moved along C_1 at forty-seven different positions (z_{tag}) by 1 cm-steps. The impedance matching of the probe is cleraly disturbed by the tag and, in particular, $|S_{11}|^2$ degrades (i.e. increases) as the tag is closer to the standing wave peak. The corresponding oscillatory behavior of the turn-on power of the tag in the considered

positions (Fig.13(b)) is thus mainly due to the impedance mismatch of the excitation probe since the power transmission coefficients of the tag are quite uniform, as demonstrated by simulations in Fig.6(b). In all cases, measurements are rather coherent with the simulations provided that a 20 MHz mutual frequency shift is accounted for, as discussed above.

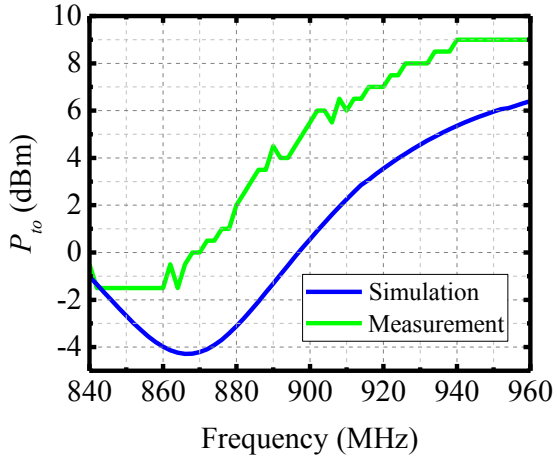

Fig. 12 : Example of measured turn-on power of a tag placed inside the cavity on cylinder C_1 in position z=10 cm and comparison with simulations.

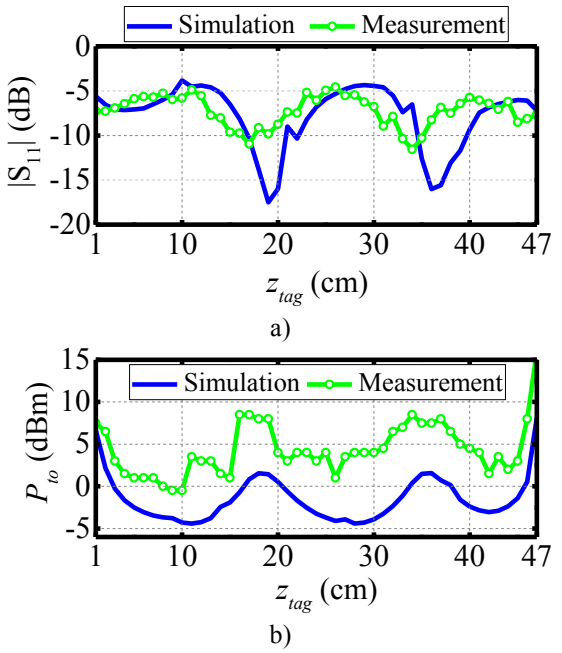

Fig.13: a) Measured and simulated reflection coefficient of the source probe (at 867 MHz) in the presence of an internal temperature sensor as it was placed over C_1 at several positions along the z-axis. b) Measured and simulated turn-on powers of the tag in the same conditions as above and accounting for a 20MHz frequency shift as in Fig.12.

B. *Simulatneous four tags in different displacements*

Three configurations of sensor network are finally tested by placing four tags inside the cavity in different positions as in Fig. 14 concerning both the inter-element spacing and the angular displacement. The tags are placed so that the tag n=4 is the closest to the source probe and the tag n=1 the farthest.

Unlike simulations, the experimental distribution of the turn-on powers (Fig. 14) is rather uniform along the alignment of sensors and is sensitive to the specific arrangement. The worst configuration, both in terms of the peak value, the average turn-on power and of its variability, occurs with the smallest inter-tag distance (Conf. B), as confirmed by simulation. The other two arrangements, corresponding to aligned and alternated sensors placed at a mutual larger distance, exhibit instead lower and similar power distributions. Overall, the average difference between the measured and simulated data is 3.9 dB.

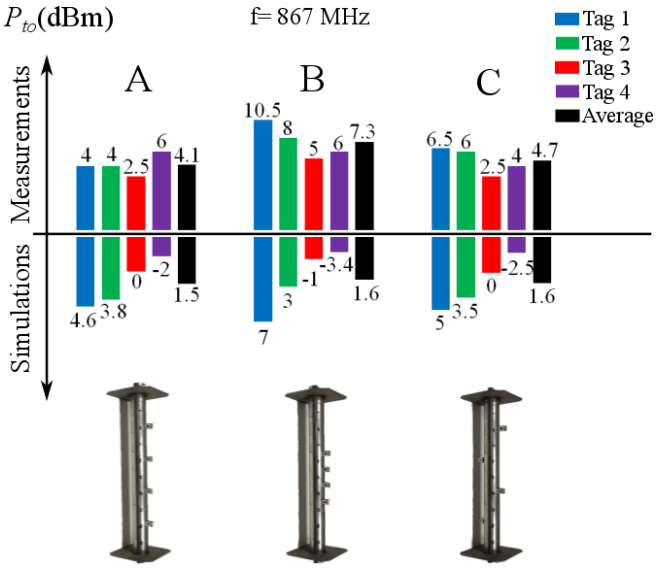

Fig. 14: Diagram of the turn-on power (dBm) measured at 867 MHz for the four prototypes in the configurations A, B and C, and the turn-on power of a single tag in the same positions, (A', B' and C').

V. Examples of Temperature Measurements

Some preliminary experiments of temperature measurement inside the mockup were performed by using the RADIOSCAN Kit [21] according to the set-up of Fig. 15. To artificially generate an internal temperature gradient, hot air was flushed inside the mockup by using a hair dryer.

A. *Aligned sensors*

In a first test, hot air flow was directed into the hollow metallic cylinder C_1 from the right side of the structure. To emphasize the heating effect, the circular aperture in the left cap of the smaller cylinder C_1 was closed by aluminum tape (Fig.15). It is worth noting that this arrangement does not perturb the boundary conditions of the coaxial enclosure that is still decoupled from the interior of C_1, and accordingly the RFID link is the same as that previously considered throughout the paper.

Four sensors were placed along and over C_1 in the configuration A (Fig. 16(a)). Consequently, the cylinder increased its temperature from right (tag 4) to left (tag 1). Thus, tag n.4 was the first one to reach the maximum temperature detectable by the EM4315 chip (63.25 ºC), quickly followed by tags n.3, n.2 and n.1. After 10 minutes of low temperature variations due to low heating and cooling cycles, the temperature increased rapidly (Fig. 16.(b)) and then the mock-up was left at room temperature for the cooling cycle.

A. Interleaved sensors

In the second experiment, the sensors were placed according to configuration C. The air flow is introduced between the cylinders C_1 and C_2 by a narrow slit opened in the rim of right cover for that purpose (Fig. 17(a)). Also in this case the RFID link is expected not to undergo significant changes.

The temperature values of the four sensors vs. time are displayed in Fig. 17(b). At time t= 0 s, the hot air flux is hitting directly tag n.3, so that it is the first sensor to reach the maximum temperature followed by tag n.1. Tag n.4 and tag n.2 are in the opposite side of C_1, so the hot air flux doesn't hit them directly and therefore they detect temperature increase more slowly. A snapshot of temperature distribution superimposed to the scene at time t = 250 s is visible in Fig. 17(b). Then, at time t = 800 s, the angle of the air flux was changed hitting directly tag n.1, which thus reached the maximum temperature faster than tag n.3, as it can be noticed from the different slopes of the temperature profiles.

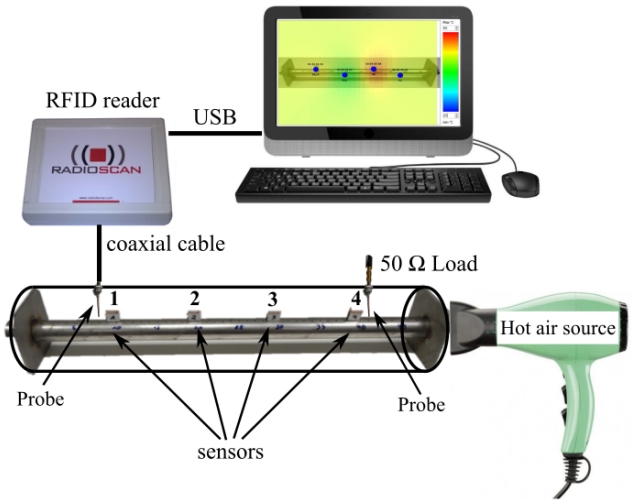

Fig. 15: Temperature measurement set-up consisting of: a hot air source producing a temperature rise, the cavity mock-up, four sensors, the load probe connected to a 50 Ω resistor, the source probe connected to the RadioScan reader by a coaxial cable. The reader is then connected to a computer, by means of a USB cable, where the collected data can be stored, visualized and processed. Sensors are placed as in configuration A and C.

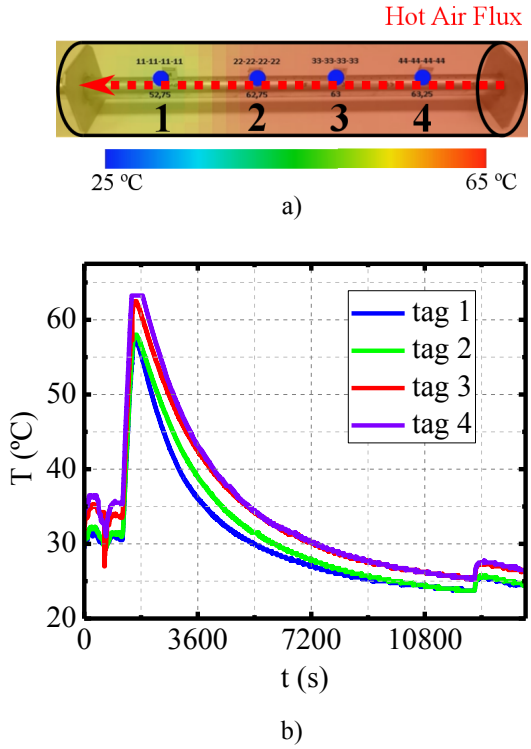

Fig. 16: a) Snapshot of the temperature distribution inside the camera as spatial interpolation of the data sampled by the sensors in case of hot air flushed inside C_1 from the right side while the left side was closed b) Transient temperature response of the four sensors.

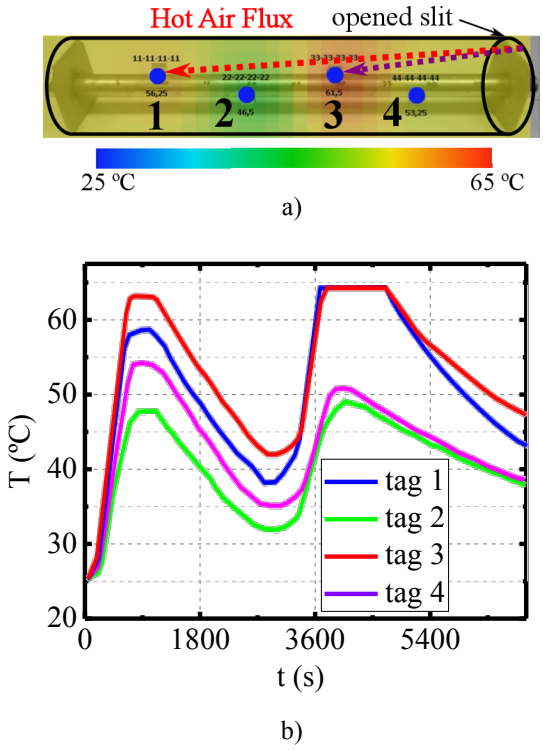

Fig. 17: a) Snapshot of the temperature distribution inside the camera at time t = 250 s as spatial interpolation of the data sampled by alternating sensors in case of hot air flushed inside C_2 through the opened slits in the C_2 right lid. b) Transient temperature response of the four sensors.

VI. Discussions and Conclusions

This contribution has proved that a passive RFID network can be used to measure the time-variant temperature inside a coaxial cavity, resembling a Cyclotron Auto-Resonance Maser by means of a wireless and batteryless infrastructure. Due to the small internal volume of the cavity, the internal electric field is sensibly perturbed by the presence of the tags, and the power that the reader must emit to establish the RFID communication increases with the number and density of sensors. In case of dense displacement of tags (N>16), some of them could be unreadable due to the power attenuation inside the cavity loaded with tags. A possible extension of the reading region, still to be experimentally evaluated, could involve the use of both the probes in alternating interrogation mode. By using a reader with two output ports, the two cavity probes would be interrogated sequentially and cyclically. When the probe n.1 is sourced, the port n.2 is connected to the internal matched load of the reader's generator, thus acting as termination load for the cavity. The switch between the two ports can be generally controlled via software in common COTS readers, as already experimented in [23]. By using this architecture, the required reader's power is expected to be less than 20dBmW even in case of N=16 sensors, with therefore still some margin either to further increase the number of temperature sampling points or to further miniaturize the tag size. In addition, power budget is going to be reduced by using less power-hungry RFID IC sensors (like RFmicron Magnus 3 [22]) not yet available during the planning of this work.

The very still open issue concerns the cohabitation of the RFID link with possible leakage of terahertz fields inside the cooling cavity, given the specific susceptibility of the tags' microchip. Conventional RFID chips based on non-volatile memories may indeed face a significant drawback when exposed to high power and high frequency fields. After irradiation, memory content could be erased or corrupted. Moreover, in case of sensor-oriented chips, additional critical issues could be *i*) an artificial increase in the temperature due the direct warming effect of the chip itself that is exposed to radiation and *ii*) an anomalous temperature output due to the internal polarization phenomena inside the chip silicon devices. Some possible mitigation solutions have been already investigated in [24], [25], and commercial radiation resistant RFID tags are currently available on the market [26], [27]. However, a focused research with a dedicated exposure set-up is required to quantitatively study the possible artifacts and corrections of the temperature sensing in such a harsh environment and it will be the topic of a future work.

Acknowledgment

This work was supported in part by the Spanish Ministerio de Economía y Competitividad and FEDER funds under project TEC2015-69229-R.

References

[1] S. Ceccuzzi, et al, "Status of ENEA 250 GHz Cyclotron Autoresonance Maser project", *40th Int. Conf. Infrared and Terahertz Waves (IRMMW-THz-2015*, China 2015.
[2] DEMO TOKAMAK, http://www.enea.it/it/seguici/pubblicazioni/pdf-volumi/v2016-cdr-carm.pdf.
[3] C. Occhiuzzi, S. Caizzone, G. Marrocco, "Passive UHF RFID Antennas for Sensing Applications: Principles, Methods and Classifications", IEEE Antennas and Propagat. Magaz., Vol.44, N.6, pp.14-34, Dec, 2013
[4] G. Marrocco et al, "RFID & IoT: a synergic pair", *IEEE RFID Virtual Journal*, N.8, March 2015, http://ieeexplore.ieee.org/xpls/virtual-journal/virtualJournalHome?pub=rfid&issue=8
[5] S. Amendola, G. Bovesecchi, A. Palombi, P. Coppa, G. Marrocco, "Design, Calibration and Experimentation of an Epidermal RFID sensor for remote Temperature Monitoring," *IEEE Sensors Journal* , vol.16, no.19, pp.7250-7257, October 2016.
[6] J. F. Salmerón *et al*., "Design and Development of Sensing RFID Tags on Flexible Foil Compatible With EPC Gen 2," in *IEEE Sensors Journal*, vol. 14, no. 12, pp. 4361-4371, Dec. 2014.
[7] P. V. Nikitin, D. D. Arumugam, M. J. Chabalko, B. E. Henty and D. D. Stancil, "Long Range Passive UHF RFID System Using HVAC Ducts," in *Proceedings of the IEEE*, vol. 98, no. 9, pp. 1629-1635, Sept. 2010.
[8] P. V. Nikitin, D. D. Stancil, A. G. Cepni, O. K. Tonguz, A. E. Xhafa and D. Brodtkorb, "Propagation model for the HVAC duct as a communication channel," in *IEEE Transactions on Antennas and Propagation*, vol. 51, no. 5, pp. 945-951, May 2003.
[9] D. D. Arumugam and D. W. Engels, "Characterization of RF Propagation in Helical and Toroidal Metal Pipes for Passive RFID Systems," *2008 IEEE International Conference on RFID*, Las Vegas, NV, 2008, pp. 269-276.
[10] A. Nasir, Boon Hee Soong and K. A. Qaraqe, "RFID in-pipe moisture sensing system for oil and gas quality monitoring in Qatar," *2013 19th IEEE International Conference on Networks (ICON)*, Singapore, 2013, pp. 1-5.
[11] P. V. Nikitin, D. D. Stancil, O. K. Tonguz, A. E. Xhafa, A. G. Cepni and D. Brodtkorb, "Impulse response of the HVAC duct as a communication channel," in *IEEE Transactions on Communications*, vol. 51, no. 10, pp. 1736-1742, Oct. 2003.
[12] P. V. Nikitin and D. D. Stancil, "Antenna radiation resistance in waveguide and in free-space," in *IEEE Transactions on Antennas and Propagation*, vol. 53, no. 6, pp. 2126-2128, June 2005.
[13] MURATA, http://www.murata.com/products/inductor
[14] S. J. Orfanidis, ElectromagneticsWaves and Antennas [Online]. Available: http://www.ece.rutgers.edu/~orfanidi/ewa.
[15] FEKO EM Simulation software, http://www.feko.info
[16] P. V. Nikitin, K. V. S. Rao, S. F. Lam, V. Pillai, R. Martinez and H. Heinrich, "Power reflection coefficient analysis for complex impedances in RFID tag design," in *IEEE Transactions on Microwave Theory and Techniques*, vol. 53, no. 9, pp. 2721-2725, Sept. 2005.
[17] http://www.emmicroelectronic.com/products/rf-identification-security/epc-and-uhf-ics/em4325
[18] S. Amendola, G. Bovesecchi, A. Palombi, P. Coppa, G. Marrocco, "Design, Calibration and Experimentation of an Epidermal RFID Sensor for Remote Temperature Monitoring", *IEEE Sensors Journal,* Vol.16, N.19, pp. 7250-7257, 2016
[19] http://www.thingmagic.com/index.php/embedded-rfid-readers.
[20] ENEA, http://www.enea.it/it/centro-ricerche-frascati.
[21] Radio6ense: http://www.radio6ense.com/company.
[22] RFMICRON Magnus, http://rfmicron.com/magnus-family
[23] S. Amendola, C. Occhiuzzi, G. Marrocco, "RFID Sensing Networks for Critical Infrastructure Security: a real testbed in an Energy Smart Grid", 2017 IEEE RFID-TA, Warsaw (Poland), Sept. 2017.
[24] Teraura N, Ito K, Takahashi N, Sakurai K. The Development of Radiation-Resistant RF Tags for Use at Nuclear Power Plants. ASME. International Conference on Nuclear Engineering, Volume 1: Plant Operations, Maintenance, Engineering, Modifications, Life

Cycle and Balance of Plant; Nuclear Fuel and Materials; Radiation Protection and Nuclear Technology Applications ():V001T01A043.
[25] N. Teraura, K. Ito, D. Kobayashi and K. Sakurai, "Evaluation of gamma ray durability of RF tag and application to the radiation environment," 2015 IEEE International Conference on RFID Technology and Applications (RFID-TA), Tokyo, 2015, pp. 147-152
[26] G. Andrechak and R. A. Wiens, "Hitachi μ-chip RFID technology compatible with gamma sterilization," http://iiaglobal.com/uploads/documents/uChip_Gamma_White_Paper_rev5.pdf, 2018.
[27] M. Anzai, "Gamma-Resistant FRAM RFID Chips Enable Cradle-to-Grave Tracking of Medical Devices", 2013. [Online]. Available: http://www.medtecjapan.com/en/news/2012/07/10/828. [Accessed: 26-Apr-2018].

Sergio Lopez-Soriano was born in Barcelona, Spain. He received the degree in Telecommunication Engineering from the Universitat Autònoma de Barcelona (UAB), Bellaterra, Spain, in 2012, with a thesis on the implementation of a testbed for hydrogen fuel cells, as a part of the european project LoLiPEM. He received the M.Sc. degree in Micro and Nanoelectronics Engineering and the Ph.D. degree in Electronics and Telecommunication Engineering from the Universitat Autònoma de Barcelona (UAB), Bellaterra, Spain, in 2013 and 2018. In 2015, he joined the University of Rome Tor Vergata as a visiting researcher. He was involved in the study, design, manufacturing and evaluation of a passive wireless sensor network for temperature mapping inside a shielded enclosure, as a part of the CARM project carried out in ENEA.

Ivan Spassovsky received the M.Sc. degree and later the Ph.D degree in physics from Sofia University, Bulgaria. He then joined the department of General Physics, the laboratory of Plasma Electronics where his research has focused on the physics of intense electron beams and their applications in coherent radiation sources. In 1992 he moved to the Brazilian Institute of Space Research(INPE) where he participated the research on 28 GHz Gyrotron. In 1994-1995 he joined the ENEA, Frascati FEL team and work on development of compact microtron driven FEL. He spent two years with the Korean Atomic Energy Institute (KAERI) collaborating in the realization of Far-Infrared FEL. In 1999 he moved to the University of Maryland, Colleague Park where he participated in second harmonic Gyroklystron Project developing advance driver for next generation Linear Colliders. In 2002 he returned to ENEA, Frascati, Italy. He worked on the compact IR FEL and SPARC Free Electron Lasers . Currently he is responsible for development of 250 GHz CARM oscillator for plasma heating in TOKAMAK Fusion Reactors at the Fusion Department.

Josep Parrón received the Telecommunication Engineer degree and the Doctor Engineer degree from the Universitat Politècnica de Catalunya (UPC), Spain, in 1994 and 2001, respectively. Since 2002, he has been an Associate Professor in the Telecommunication and Systems Engineering Department, Universitat Autònoma de Barcelona (UAB), Spain. His research interests include numerical methods for electromagnetism, antenna design and phased arrays. He is the author or coauthor of more than 80 technical journal articles and conference papers.

Gaetano Marrocco Laurea and the Ph.D. in Applied Electromagnetics from the University of L'Aquila, Italy, in 1994 and 1998, respectively. Researcher at the University of Roma Tor Vergata in 1994-2014. Associate Professor of Electromagnetics in 2013-2017. Guest Professor at the University of Paris-est Marne la Vallèe in 2015 and Full Professor at the University of Roma Tor Vergata since 2018.

His research is mainly directed to the modelling and design of broadband and ultra wideband (UWB) antennas and arrays as well as of sensor-oriented miniaturized antennas for Biomedical Engineering, Aeronautics and Radiofrequency Identification (RFID). During the last decade, he carried out pioneering research on the wireless-activated sensors, contributing to move from the labeling of objects to the passive sensor networks in the Internet of Things era. He serves as Associate Editor of the IEEE Journal of Radiofrequency Identification and member of the IEEE Antennas and Propagation Society Awards committee. He is moreover Vice-Chair of the Italian delegation URSI Commission D Electronics and Photonics. He was the chair of the Local Committee of the V European Conference on Antennas and Propagation (EUCAP-2011), TPC chair of the 2012 IEEE-RFID TA in Nice, France, TPC track-chair of the 2016 IEEE Antennas and Propagation Int. Symposium, TPC track-chair of IEEE-RFID 2018 USA.

Prof. Marrocco is the chair of the Pervasive Electromagnetics Lab and the co-founder and president of the University spin-off RADIO6ENSE (www.radio6ense.com) active in the short-range electromagnetic sensing for Industrial Internet of Things, Smart Manufacturing, Automotive and Physical Security.